Characterization of some Low Spin Complexes of Ferric Hemeoctapeptide From Cytochrome-*c*

JOHN W. OWENS*, CHARLES J. O'CONNOR

Department of Chemistry, University of New Orleans, New Orleans, La. 70148, U.S.A.

and RICHARD D. KASSNER

Department of Chemistry, University of Illinois at Chicago, Chicago, Ill. 60680, U.S.A.

(Received June 25, 1987)

Abstract

Complexes of hemeoctapeptide, derived from bovine cytochrome *c*, show similar magnetic properties to those of low spin complexes of cytochrome *c* and hemoglobin. The electronic properties of hemeoctapeptide and cytochrome complexes are also similar while the Soret and beta bands of these analogs are generally blue shifted from those of corresponding complexes of hemoglobin due largely to the differences in the type of heme. Electron spin resonance calculations were carried out using Taylor's method to elucidate d orbital splittings and structural differences in hemeoctapeptide, hemoglobin, and cytochrome *c*. A correlation between *V*, the rhombicity, and the position of the beta band was found to exist and was dependent on protein type. However, neither the electronic nor magnetic data was largely dependent on protein bulk. A large rhombic splitting caused shifts to the blue, and showed a dependence of the porphyrin pi orbitals on the placement of the metal relative to the porphyrin plane. A structural basis for the degree of rhombic splitting and thermodynamic parameters for ligand binding is proposed.

Introduction

The hemeoctapeptide derived from cytochrome *c* by enzyme hydrolysis has been used as a model for several heme proteins, including hemoglobin and cytochrome *c* [1–9], even though the biochemical processes that these proteins participate in are quite different. The active site of hemoglobin is known to be centered on the heme iron, while works by Gray [10], Sykes and coworkers [11], and McClendon and Smith [12] have shown that the reactivity of cytochrome *c* is centered on the heme edge. Because the hemeoctapeptide is a smaller system, yet maintains a partial peptide heme environment including axial coordination of a histidyl imidazole group to the heme iron, it is better suited than hemin as a model of more complex heme proteins. The hemeoctapeptide molecule is illustrated in Fig. 1.

McLendon and Smith [8] reported that the rate constants for electron transfer between a pyridyl ruthenium complex and the hemeoctapeptide were: (1) faster in the peptide than in cytochrome *c*, and (2) independent of the nature of the ligand. Stereochemical accessibility of the active site in the model compared to the bulkier parent protein was reported to cause the faster rates. McLendon and Smith also reported that ligand addition was faster for the hemeoctapeptide than for myglobin. The difference in rates was attributed to the thermodynamics of protein rearrangement.

While these studies suggest differences in the reactivity of the hemepeptide and hemoglobin and/or cytochrome-*c* associated with protein bulk, there are other reports which show that the band positions for ESR and UV–Vis spectra are affected only slightly

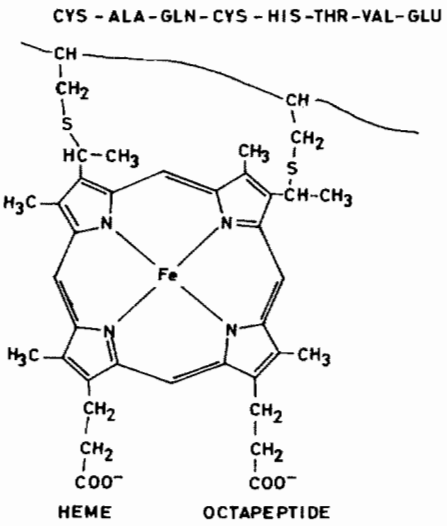

Fig. 1. Structure of the ferric hemeoctapeptide molecule showing the peptide chain attached to the porphyrin through the cysteine linkages. The histidyl imidazole is also attached to one axial position of the iron.

*Current address: Department of Chemistry, Southern University, Baton Rouge, La. 70813, U.S.A.

0020-1693/88/$3.50

by differences in protein bulk [9, 10, 13]. It appears that in the case of hemeoctapeptide, there are significant kinetic and thermodynamic differences between the model and parent cytochrome, but the electronic and/or magnetic properties remain similar.

Electron spin resonance has been used extensively to gather information about the crystal field properties of low spin hemoproteins. Griffith developed the first such model for hemoglobin azide [18]. Blumberg and Peisach [21–22] have characterized many proteins according to their rhombic/-tetragonal content. Harris [19], Salmeen [17], and Taylor [14] simplified Griffith's model. Iwaisumi and Migita [16], and Salermo and Leigh [15] have shown the usefulness of this model with tetraphenyl porphyrins. Recently Muhoberac presented another variation of Griffith's model for cytochrome-*c* complexes [20].

This report further describes the electronic and magnetic properties of hemeoctapeptide and its complexes and compares them to hemoglobin and cytochrome-*c* and their complexes. These comparisons provide information about differences in the structural geometry of the binding and/or active site, which are relevant to the use of hemeoctapeptide as a suitable model for these hemoproteins.

Experimental

Spectroscopy

The UV–Vis spectra were obtained with the CARY model 17 spectrophotometer using cells of 1 cm path length. The hemeoctapeptide complexes were maintained at a concentration of 8.3×10^{-5} M except in the Soret region where the concentration was lowered to 8.3×10^{-6} M. The hemeoctapeptide complexes were prepared in a 50/50 volume/volume 40 mM phosphate buffer – ethylene glycol, maintained at a pH of 7.2. Hemeoctapeptide was prepared following published procedures [2–4].

Electron Spin Resonance

The ESR studies were obtained using a Varian-E3 Spectrometer operating at X-band and equipped with either a Varian liquid nitrogen temperature (77 K) device or an Air Products helitran (4K). The hemeoctapeptide complexes were prepared at a concentration of 8.5×10^{-5} M, bubbled with nitrogen and transferred to capped quartz tubes for study. Only the hemeoctapeptide was examined in the solid state. All of the complexes were monitored at 20 degree intervals from 300 to 80 K via the liquid nitrogen variable temperature device, then transferred to the Helitran cyrostat to obtain information at 4 K. ESR g values were determined by comparison with DPPH, $g_1 = g_2(H_2/H_1)$. The magnetic field calibration was periodically checked using both DPPH and a gauss meter.

Magnetic Susceptibility

Temperature dependent magnetic susceptibility of solid hemeoctapeptide was measured using both an Alternating Force Magnetometer (AFM) and the S.H.E. Corp. superconducting SQUID susceptometer. Measurements were recorded over the temperature range 300 to 6 K. Samples for study were weighed and sealed in a teflon bucket (AFM) or Si/Al alloy bucket (SQUID). Measurement and calibration techniques are reported elsewhere [35].

Results

A table of the UV–Vis data and extinction coefficients is presented in Table I. Figures 2 and 3 show spectra for typical high and low spin hemeoctapeptide complexes, respectively. Typical high spin

TABLE I. Electronic Transitions for Ferric Hemeoctapeptide Complexes (nm)[a]

Ligand	N	L	Soret	Beta (hs)	Beta (ls)	Alpha	CT[b]
Alone	260	355	398	495	532	565	622
	15.0	35.1	141.0	6.85	5.09	3.63	3.18
Azide		351	410		533	567	622
		27.5	113		8.65	5.08	1.57
Pyridine		354	404		525	555	
		22.5	110.1		9.02	6.65	
Imidazole	262	348	406.5		528	557	
	25.0	26.1	116.0		9.59	7.24	
Cyanide	265	353	412		533		
	26.1	27.8	99.8		9.76		

[a]All spectra were done at 300 K for the range 200–750 nm. Extinction coefficients are in mM^{-1} cm^{-1}. The solvent is a 50/50 *v/v* 40 mM phosphate buffer–ethylene glycol mixture. Some band positions and extinction coefficients were reproduced from ref. 2. [b]CT refers to charge transfer bands. There are bands occurring toward the near infrared which have been assigned to d–d transitions, charge transfer transitions, and even mixing of these with the porphyrin ring pi transitions (see refs. 23–24).

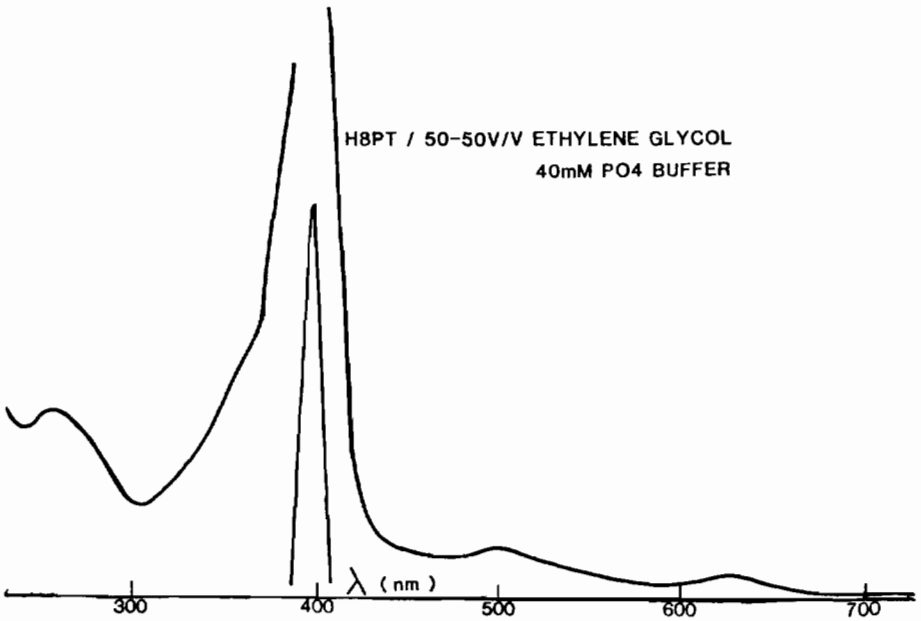

Fig. 2. UV–Vis spectrum of high spin hemeoctapeptide in ethylene glycol/buffer solution.

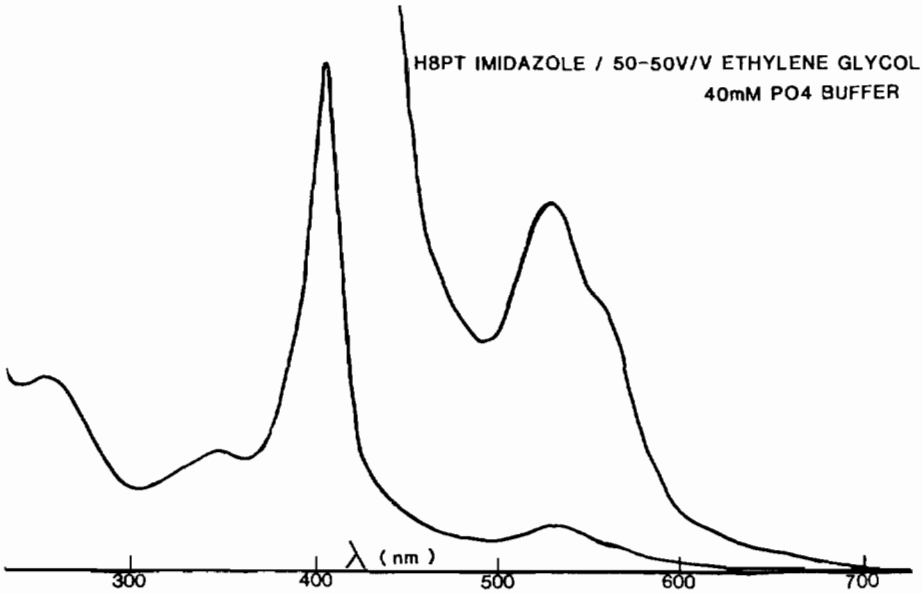

Fig. 3. UV–Vis spectrum of low spin hemeoctapeptide-imidazole in ethylene glycol/buffer solution.

ferric complexes exhibit prominent peaks near 500 and 625 nm in the visible region of the spectrum whereas low spin complexes exhibit prominent bands near 540 and 570 nm.

Electron spin resonance data for some high and low spin hemeoctapeptide complexes are presented in Table II. Figure 4 illustrates ESR spectra for the low spin H8PT-imidazole complex. High spin complexes which are tetragonally distorted exhibit ESR g values at 6.0 (strong) and 2.0 (weak), where the value at 6.0 is associated with electron resonance in the xy plane and the value at 2.0 is associated with resonance along the z axis. The z axis is normal to the plane of the porphyrin ring. The g tensor for the low spin complexes requires three g values centered around 2.0, that result from the rhombic geometry. According to Blumberg's rules [25], these three g values are assigned as g_z (highest), g_y, and g_x (lowest).

The two high field g values for the hemeoctapeptide (H8PT) cyanide complex were not resolved at 4 K. g_y, which exhibited a peak width of about 40 gauss, was estimated from the weight of the distribution of the trough and g_x was calculated from Bohan's equation [26]:

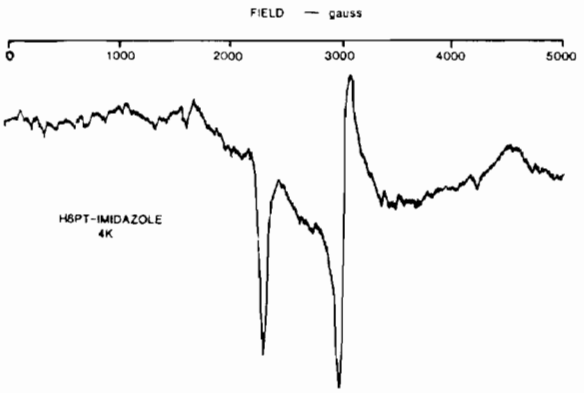

Fig. 4. ESR spectrum of low spin H8PT-imidazole recorded at 4 K.

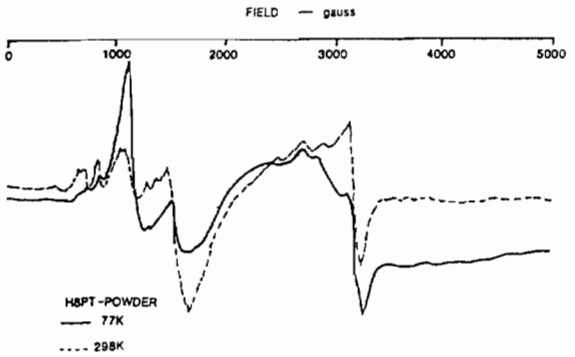

Fig. 5. ESR spectra of H8PT powder at 298 and 77 K. The presence of the dimer is indicated by the peaks at $g = 4.0$ and 2.0.

$$g_x^2 + g_y^2 + g_z^2 - g_x g_z - g_y g_x + g_y g_x - 4g_x - 4g_y + 4g_z = 0 \quad (1)$$

The g values are similar to those reported by McLendon and Smith [12].

The electron spin resonance spectrum obtained for the hemeoctapeptide powder exhibited a series of high and low field peaks with the most prominent occurring near $g = 6.0$, 4.0, and 2.0. The ESR spectrum for the powder was surprising because it was expected to be exclusively high spin (see Fig. 5). The hemeoctapeptide has been characterized as having a water molecule attached to the second axial site. Both methemoglobin and metmyoglobin also have water molecules opposite the amino acid linked histidine unit. Both of these proteins have been universally characterized as high spin. The behavior of the H8PT is not unusual for powders, however, the positions of the high and low field peaks remained essentially unchanged across the temperature range 298–77 K. The ESR spectrum is most consistent with a system of approximately 50/50 monomer/dimer heme. The monomer is identified by the $g = 6.0$ value, and the dimer by the $g = 4.0$, and 2.0 values. The dimerization may be caused by lyophilization of the peptide during preparation. The ESR spectrum provided no evidence for the presence of a low spin component for the H8PT powder. Likewise, ESR spectra of the H8PT in buffer solution exhibited an exclusively high spin behavior across the temperature range 298–4 K, with no evidence of dimerization. However, the UV–Vis spectra of this same solution also suggested a mixed high spin/low spin complex with typically well characterized bands occurring at 494, 532, 565 and 622 nm. The bands near 500 and 622 nm are associated with the high spin component while the band at 560 nm is associated with the low spin component. The band at 532 nm is a mixture of both components. These observations suggest that the hemeoctapeptide in solution is of mixed spin state consistent with earlier work by Huang and Kassner [5] based on NMR measurements.

The magnetic moments for the hemeoctapeptide powder were calculated from susceptibility measurements to be 2.74, 2.51, and 2.24 at 298, 77 and 4 K, respectively with magnetic susceptibility values of 0.003137, 0.01020 and 0.10499 e.m.u./mol. The magnetic moments correspond to low spin iron with either significant orbital contributions at the higher temperatures with mixing of excited states into the ground state, or more likely dimerization.

TABLE II. ESR g-Values for Complexes of H8PT[a]

Compound	4 K
Alone	5.57, 2.06
Cyanide	3.34, 1.80 (estimated), 1.01
Imidazole	2.84, 2.15, 1.51
Azide	2.78, 2.14, 1.70
Pyridine	3.20 (others unresolved)

[a]The solvent is a 50/50 v/v solution of ethylene glycol–40 mM phosphate buffer (pH = 7.2).

Discussion

For high spin ferric complexes, several bands are distinctive. The Soret band (also known as the B band) is found near 400 nm, and the alpha/beta (Q_o, Q_v) bands, occurring near 540 and 500 nm, respectively, are associated with the porphyrin $\pi \rightarrow \pi^*$ transition (a_{1u}, $a_{2u} \rightarrow e_g(\pi^*)$ (see Fig. 6)). The alpha band is less intense, and is usually seen as a shoulder of the beta band, which is able to gain intensity through vibronic coupling with the very intense Soret band. The B(1, 0) component of the Soret band occurs approximately 20–30 nm to the blue of the B band, and is seen as a shoulder. Low spin complexes

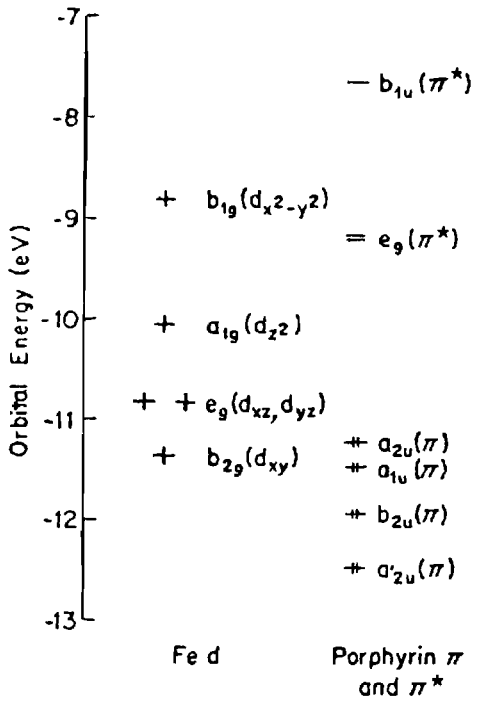

Fig. 6. Molecular orbital diagram of iron(III) in a porphyrin environment.

exhibit alpha/beta bands at about 575 and 540 nm, respectively, which are usually well resolved. However, when the axial ligands are good pi acceptors like cyanide or imidazole, the beta band is so intense that the weaker alpha band may not be visible or appears as a shoulder of the α peak. The enhanced resolution of the alpha/beta for many low spin complexes compared to that for high spin complexes has been associated with the removal of degeneracy of the $e_g(\pi^*)$ in low spin compounds [36]. The red shift of alpha/beta bands in low spin ferric heme complexes has been attributed to configuration interaction [30]. The band at 350 nm (N band) is derived from heme a_{2u}', $b_{2u} \rightarrow e_g(\pi^*)$ transitions.

Charge transfer transitions are also present in the visible region [24]. High spin complexes exhibit these bands near 580 and 630 nm, derived from a_{1u} and $a_{2u} \rightarrow d_{xz}, d_{yz}$(por $\rightarrow$ metal) transitions, respectively. These transitions are usually unresolved in low spin complexes, with a single band of mixed $a_{1u}, a_{2u} \rightarrow d_{xz}, d_{yz}$ transitions shifting to 1300 nm in the IR. Other charge transfer bands occur in the ultraviolet and near infrared [37, 39], but will not be discussed in this paper. The positions of the charge transfer bands are dependent on both the nature of the ligand, and on the oxidation state of the metal. Low spin ferric complexes seldom display CT bands between 600–800 nm. However, if both low and high spin forms are present, the high spin form may be evident in this region. Charge transfer bands occurring near 488 and 340 nm have been identified and assigned on the basis of PR data [36–39] for both low and high spin complexes. However, since they are usually *z* polarized (and therefore of low intensity) they are often buried beneath the more prominent bands.

Table I shows that as the ligand becomes a better pi acceptor, the position of the Soret band is shifted to the red. This band shifts from 398 nm for aquo hemeoctapeptide to 404 for the pyridine complex to 412 for the cyanide species [27]. As the metal e_g–t_{2g} separation increases on going from a high to a low spin state, the porphyrin ring $a_{1u}, a_{2u} \rightarrow e_g$ pi orbital energy separation decreases, primarily through an increase in the energy of the a_{1u} and a_{2u} orbitals [24]. Gouterman's calculations show a sequential increase in both the energies of the a_{1u} and a_{2u} ring orbitals and the metal $e_g(d_{xz}, d_{yz})$ orbitals, with only a slight increase in the energy of the porphyrin ring e_g^* orbital, as the ligand field is varied from high to low spin.

The blue shift of the Soret for high spin complexes may also be due to perturbation of porphyrin π orbitals brought on by the removal of the iron from the plane of the porphyrin ring [36].

The quantification of the tetragonal, rhombic, zero field splittings, and orbital energies was accomplished using the method of Taylor [14]. According to this method, the d orbitals are arranged as in Fig. 7, where only a perturbation of the t_{2g} orbitals (d_{xy}, d_{xz}, d_{yz}) is shown as the symmetry of the molecule is lowered. This method assumes that the e_g orbitals $(d_{z^2}, d_{x^2-y^2})$ are completely isolated from the t_{2g} set. Under octahedral symmetry all three t_{2g} orbitals are degenerate. When there is an axial distortion and the symmetry is lowered, this degeneracy is removed and the d_{xy} orbital is lowered in energy while the d_{xz} and d_{yz} orbitals are raised in energy, assuming a positive axial distortion.

The energy separation between the doubly degenerate d_{xz}, d_{yz} set and the d_{xy} orbital is called the tetragonal splitting. If there is a further lowering of the symmetry by an in-plane mechanism, the symmetry of the system is lowered from D_{4h} to

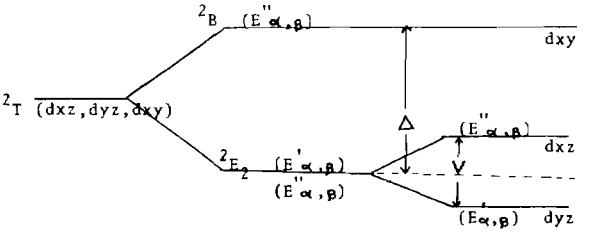

Fig. 7. One hole model representing the splitting of the d-orbitals under octahedral cubic, tetragonal, and rhombic distortions. *V* represents rhombic splitting, and Δ represents tetragonal splitting.

D_{2h} which removes the degeneracy of the d_{xz} and d_{yz} orbitals. The energy separation between the d_{xz} and d_{yz} orbitals is called the rhombic splitting, V. The electronic configuration of such a ferric porphyrin complex is $d_{xy}^2 d_{xz}^2 d_{yz}$. Because the tetragonal, rhombic, and spin orbit coupling operators are nonzero for a T configuration, the three orbitals of the t_{2g} set can mix. According to Taylor's one hole notation, the mixing of these three t_{2g} orbitals form a molecular orbital pair represented by:

$$|+\rangle = a|d_{yz}^{+}\rangle - ib|d_{xz}^{+}\rangle - c|d_{xy}^{-}\rangle$$
$$|-\rangle = -a|d_{yz}^{-}\rangle - ib|d_{xz}^{-}\rangle - c|d_{xy}^{+}\rangle \quad (2)$$

where a, b and c are the coefficients of mixing. When the Zeeman operator is applied to these two wavefunctions, the relationship between the coefficients and the principal g values is obtained:

$$a = (g_z + g_y)/4p$$
$$b = (g_z - g_x)/4p \quad (3)$$
$$c = (g_y - g_x)/4p$$

where $p = (g_z + g_y + g_x)/2$

This result assumes that the product $g_z g_y g_x$ is positive for $a = 1.0$ and that there be no covalent bonding. Taylor's method therefore is a first order approximation of the energies of these orbitals. Once the coefficients are determined, they may be used to obtain the energies of the d_{xz}, d_{yz}, and d_{xy} orbitals by solving the determinant below.

$$\lambda \cdot \begin{bmatrix} 0 & i/2 & -i/2 \\ -i/2 & -A & i/2 \\ -i/2 & -i/2 & -B \end{bmatrix} \cdot \begin{bmatrix} a \\ -ib \\ -c \end{bmatrix} = E \begin{bmatrix} a \\ -ib \\ c \end{bmatrix} \quad (4)$$

Three secular equations are derived from the solution to this determinant:

$$A = E(d_{xz}) = g_x/(g_z + g_y) + g_y/(g_z - g_x)$$
$$B = E(d_{xy}) = g_x/(g_z + g_y) + g_z/(g_y - g_x) \quad (5)$$
$$E = E(d_{yz}) = g_x/(g_z + g_y) - \tfrac{1}{2}$$

The energies are in units of λ, the constant of the spin orbit coupling.

The degree of rhombic splitting increases in the following order (Table III): H8PT cyanide < imidazole < azide, but the tetragonal splitting is less well defined: H8PT imidazole, cyanide < azide.

The azide complex exhibits a large rhombic and tetragonal splitting, while the better pi acceptors, imidazole and cyanide, exhibit smaller splittings. These effects are explained by the mixing coefficients. While the cyanide complex shows significant mixing of the d_{xz} and d_{yz} orbitals, the azide complex has the unpaired electron spin density centered almost entirely on the d_{yz} orbital. The increased mixing of the d_{xz} and d_{yz} orbitals is evidence for a retrobonding effect between the pi orbitals of the metal and the cyanide ligand. This suggests a large crystal field splitting and subsequent stabilization of the metal pi orbitals. Likewise, the large tetragonal and rhombic splitting for the azido peptide indicates decreased crystal field splitting and a large electrostatic repulsion interaction of the pi orbitals of the metal and the azide ligand.

TABLE III. The Crystal Field Parameters for Hemeoctapeptide Orbital Energy[a]

Compound	$E(d_{xz})$	$E(d_{xy})$	V	Δ	E_1	E_2	V/Δ
H8PT cyanide	1.00	3.93	388	1575	388	1188	0.246
H8PT imidazole	1.92	4.74	768	1512	768	744	0.508
H8PT azide	2.33	6.66	931	2198	931	1267	0.423

[a]The calculations were carried out for the g-values in Tables IV and V. The energies of the orbitals are in units of λ, the spin orbit coupling constant. The splittings are in units of cm^{-1}, using a spin orbit coupling constant of 400 cm^{-1}. E_1 and E_2 are the first $\{E(d_{xy}) - E(d_{xz})\}$ and second $\{E(d_{xz}) - E(d_{yz})\}$ zero field splittings.

TABLE IV. Calculation of the Mixing Coefficients and Maximum Unpaired Spin Density

Compounds	g-Values	Mixing coefficients			Maximum unpaired spin density
		A	B	C	
H8PT cyanide	3.34, (1.80), 1.01	0.891	0.405	0.137	d_{yz}, d_{xz}
H8PT imidazole	2.84, 2.15, 1.51	0.946	0.252	0.121	d_{yz}
H8PT azide	2.78, 2.14, 1.70	0.969	0.213	0.087	d_{yz}

The binding of azide to ferric heme is different from that of both imidazole and cyanide. While ligands such as imidazole exert positive *trans* effects, presumably because the ligands bind at ninety degrees to each other, and are able to utilize different pi orbitals for retrobonding [28], cyanide always binds to iron porphyrins in such a way that its linear geometry is preserved [29]. Azide is known to bind to ferric heme in a bent arrangement [30]. The unusually large crystal field parameters for the azide peptide may therefore result from a unique bonding geometry.

The origin of the rhombic splitting in these complexes has been attributed to the placement of the metal and the histidyl imidazole relative to the porphyrin plane [31–32]. However, the greater rhombic splitting for imidazole and azide may also be associated with a preferred orientation of the bound ligand due to bonded or nonbonded interactions between the ligand and the side chains of amino acid residues in the proteins. Previous studies have indicated that hydrogen bonding or electron donor–acceptor interactions between anionic ligands and the distal histidine in hemoglobin and myoglobin may contribute to the orientation and thermodynamics of binding [33]. In cytochrome *c*, ligand binding involves displacement of the protein bound methionyl sulfur which may lead to nonbonded steric interactions which determine the orientation of the ligands.

A perfectly rhombic system would show a maximum rhombic/tetragonal splitting ratio of 0.667, meaning that the rhombicity may never be more than two-thirds the tetragonality. The separation between the three orbitals of the imidazole species is nearly equal. This is consistent with a system approaching maximum rhombicity. The rhombic/-tetragonal ratio of 0.508 is the highest for the series of complexes studied (Table III). If retrodative bonding is reflected in a decreased rhombic splitting, as in the cyanide complex, and if electrostatic repulsion is reflected in an increased tetragonal splitting, as in the azide complex, it appears that the bonding of imidazole to iron porphyrins presents pi bonding effects of both retrodative bonding and electrostatic repulsion. Buchler [34] has reported that the pi orbitals of imidazole and pyridine are both electrostatic and retrobonding, and that the strength of the bond between these ligands and iron porphyrins lies in the comparatively strong sigma bonding. Our results support such a conclusion.

A measure of the pi acid character is obtained from the variation in the mixing coefficients from the ideal value of unity, $1-(a^2+b^2+c^2)$. Taylor's method assumes that $a = 1.0$, however, because the sum of the coefficients do not add up to unity, some covalency may exist. If it is assumed that the greater the variation from unity the larger the covalent effects, the cyanide complex shows the most covalent character. Imidazole exerts the lest effect on the structure of the proteins with rhombic/tetragonal ratios approaching 0.67.

Muhoberac [20] has shown that: (1) Δ and V decrease as the e_g–t_{2g} separation increases, (2) V and Δ decrease as the pK_a of the ligand increases, (3) the electron sharing is best measured by E and V; as E decreases, V decreases and unpaired electron sharing among the d_{yz} and d_{xz} orbitals increases, (4) a greater electron sharing, smaller V is indicative of a greater pi acceptor ability, and (5) as the e_g–t_{2g} separation increases, spin orbit coupling increases for the low spin hemoproteins.

Table V shows a correlation between V, and the positions of the Soret and alpha/beta bands. These bands shift significantly to the red as the protein type changes from hemeoctapeptide to hemoglobin (as V increases) for all the low spin complexes, with much smaller shifts on going from hemeoctapeptide to cytochrome *c*. The red shift of the Soret, alpha and beta bands is greatest low spin complexes of hemoglobin. This suggests a dependence on structure between *b* and *c* type derivatives. This conclusion is supported by the similarity of the band positions for similar complexes of hemeoctapeptide and cytochrome *c*. The beta band is shifted to the blue, more so for the relatively bare hemeoctapeptide than for the bulkier hemoglobin and cytochrome *c* complexes. There is a correlation between V and the position of the beta band for similar low spin complexes of hemeoctapeptide and cytochrome *c*. This band shifts about 1–2 nm to the red for approximately every 100 cm^{-1} increase in V. However, this band may shift as much as 7 nm for rhombic changes as small as 10–15 cm^{-1} when the type derivatives are compared to similar hemoglobin complexes (*b* type derivatives). The dependence of the maxima and V on heme structure is readily understood in terms of the electronic differences between the substituents at the 2 and 4 positions of the porphyrin for the *b* and *c* type hemes. In heme *b*, the porphyrin is characterized by vinyl ($-CH=CH_2$) groups at these positions while in heme *c*, the porphyrin has thioether ($-CHSRCH_3$) groups at these positions resulting from the covalent attachment between the porphyrin and the protein. Such differences have been observed to significantly influence the position of the porphyrin and heme absorption maxima and may likewise be expected to influence the rhombic splitting. The larger rhombic splitting for the cytochrome *c* complexes containing the same heme as the hemeoctapeptide may be attributed to additional structural differences as discussed below.

The effects of axial ligands on the pi orbitals of the porphyrin ring are clearly evident in low spin complexes. The Q bands (alpha, beta) are derived from the porphyrin $\pi \rightarrow \pi^*$ transitions. Gouterman's

TABLE V. Comparative Parameters for H8PT[a] with other Proteins

	Cyanide	Azide	Imidazole
ESR *g*-values			
H8PT[b]	3.34, 1.80, 1.01	2.78, 2.14, 1.70	2.84, 2.15, 1.51
Hb/Mb	3.28, 1.97, 1.16[c]	2.80, 2.22, 1.72[d]	2.91, 2.26, 1.53[e]
CYTC	3.45, 1.89, 0.93	2.72, 2.24, 1.73	2.96, 2.30, 1.58

	Cyanide			Azide			Imidazole		
	V	Δ	V/Δ	V	Δ	V/Δ	V	Δ	V/Δ
Crystal Field Parameters (cm^{-1})									
H8PT[b]	388	1575	0.250	931	2198	0.423	768	1512	0.508
Hb/Mb	460	1480	0.311	959	1896	0.506	773	1326	0.583
CYTC	468	1370	0.342	1036	1762	0.588	787	1370	0.574

	Cyanide	Azide	Imidazole
Mixing coefficients (*a*, *b*, *c*)			
H8PT[b]	0.891, 0.405, 0.137	0.969, 0.213, 0.087	0.946, 0.252, 0.121
Hb/Mb	0.918, 0.371, 0.142	0.977, 0.210, 0.097	0.958, 0.256, 0.135
CYTC	0.899, 0.424, 0.162	0.976, 0.195, 0.100	0.970, 0.254, 0.133

	Cyanide			Azide		
	X (cm^{-1})	$\Delta H°$ (cal/mol)	$\Delta S°$ (e.u.)	V (cm^{-1})	$\Delta H°$ (cal/mol)	$\Delta S°$ (e.u.)
Formation thermodynamic parameters						
H8PT[b]	388[g]	−18900[g]	−30.1	931	−6250[p]	−14.7[p]
Hb	460[h]	−16400[h]	−15.8	959	−12900[i]	−18.4[i]
CYTC	468[m]	+1100[m]	+31.3	1036	−2300[l]	−1.6[l]

	Soret	Beta (hs)[a]	Beta (ls)[a]	Alpha (hs)[a]	Alpha (ls)[a]	V (1/cm)
Correlation of rhombicity (cm^{-1}) and UV–Vis band positions (nm)						
Alone						
H8PT[a]	398	495	532	532	565	
Hb[k]	405	500	540	540	580	
CYTC[n]	410		528			
Azide						
H8PT[a]	410		533		567	931
Hb[k]	417		540		575	959
CYTC[l]	410		535		576	1036
Imidazole						
H8PT[a]	407		528		557	768
Hb[k]	411		534		560	773
CYTC[l]	405		529		560	787
Cyanide						
H8PT[a]	412		533			388
Hb[k]	419		540			460
CYTC[n]	413		535			468

[a]H8PT = hemeoctapeptide, Hb/Mb = hemoglobin/myoglobin, CYTC = cytochrome *c*. hs = high spin component; ls = low spin component. In the case of mixed spin states, the alpha band of the high spin component overlaps the beta band of the low spin components, and occur at the same position in the visible portion of the spectrum. [b]This work. [c]Ref. 22. [d]Ref. 32. [e]Ref. 42. [f]Ref. 43. [g]Ref. 2. [h]Ref. 40. [i]Ref. 44. [k]Ref. 23a. [l]Ref. 45. [m]Ref. 46. [n]Ref. 47. [p]Ref. 4.

extended Huckel calculations show that an increased e_g–t_{2g} separation has the effect of raising the energy of the a_{2u} and a_{1u} porphyrin orbitals [24a]. Thus, a good pi acceptor like cyanide should cause a red shift of the B(Soret) and Q bands. Tables I and V support this conclusion. ESR calculations suggests that this red shift is related to decreasing rhombicity and increased sharing of the unpaired electron spin density. The final result is an increased perturbation of the porphyrin a_{2u} and a_{1u} orbitals. The effects of the metal d orbital splitting on the position of the charge transfer bands has been well established [36–

39]. These effects have been traced to the nature of the ligand. Eaton and Hochstrasser have clearly demonstrated a removal of degeneracy of the porphyrin $e_g(\pi^*)$ orbitals for complexes with tetragonal splitting. In such complexes, the alpha/-beta bands are well resolved. When the rhombic and tetragonal splitting is small, as in cyanide complexes, only the beta band is clearly discerned in normal UV–Vis spectra. These facts suggest that the ligand effects both the orbital energies and the structure of the porphyrin ring.

The thermodynamic parameters for ligand binding to the hemeoctapeptide and proteins do not appear to exhibit a general correlation with the magnetic and electronic properties. However, the data suggest that for cyanide and azide binding, rhombic and thermodynamic values may reflect the effect of structural changes in the proteins attendant to binding. The enthalpy and entropy changes increase from the H8PT to Hb to cytochrome c. While ligand binding to the H8PT is associated only with the substitution of a water molecule at the second axial position of the heme iron, the binding of cyanide to Hb [30] and cytochrome *c* is reported to result in changes in the tertiary structures of these proteins. Binding of cyanide to Hb also involves substitution of an axial water molecule but in addition involves changes in the structure of the protein associated with a steric interaction of the bound cyanide with the protein in the neighborhood of the hemes as well as distortion of the porphyrin. As previously noted, cyanide binding to cytochrome *c* involves displacement of the methionyl sulfur at the second axial position which must of necessity involve significant changes in the structure of the protein. It has earlier been suggested that the more positive ΔH° [40] and ΔS° [40, 41] changes for the proteins involve structural changes which result in a less ordered heme pocket. The corresponding increases in V may result from distortion of the porphyrin. In contrast, azide binding to Hb is reported to involve no significant changes in protein structure due to the nonlinear geometry of binding. The more negative ΔH° and ΔS° values for azide binding to Hb compared to the hemeoctapeptide has been suggested to result from the more hydrophobic environment of the heme iron and additional bonding interactions between the distal histidine and the azide in the protein. The smaller increase in V from the H8PT to Hb for azide compared to cyanide may be associated with the difference in heme type only, while the larger increase from the H8PT to cytochrome *c* for both cyanide and azide may be due to distortion of the porphyrin.

Conclusion

The similarity of the magnetic data suggests that low spin complexes of the hemeoctapeptide are good models for low spin cytochrome *c* and hemoglobin and that the magnetic data are primarily dependent on the type of axial ligands coordinated to the heme iron. Comparisons of the electronic spectra indicate that for these complexes differences between the type of heme are more important than differences in protein bulk for determining the position of absorption peaks. A correlation between the position of the absorption maxima and the rhombic splitting can in part be accounted for by the relative electronic distortion in the porphyrin by substituents at the 2,4 positions. A correlation between the thermodynamic parameters for ligand binding and the rhombic splitting is proposed to result from a distortion in the porphyrin due to changes in protein structure. The crystal field data suggest that the hemepeptide complexes may be used to further evaluate the influence of protein on rhombic and tetragonal distortion in heme protein complexes.

Acknowledgements

C.J.O. wishes to thank the Edward G. Schlieder Educational Foundation for their generous support of this research.

References

1 G. J. Hamilton, J. W. Owens, C. J. O'Connor and R. J. Kassner, *Inorg. Chim. Acta, 93,* 55 (1984).
2 R. J. Kassner and D. C. Blumenthal, *J. Biol. Chem., 255,* 5859 (1980).
3 Y. Huang and R. J. Kassner, *J. Am. Chem. Soc., 101,* 5807 (1979).
4 D. C. Blumenthal and R. J. Kassner, *J. Biol. Chem., 254,* 9617 (1979).
5 Y. Huang and R. J. Kassner, *J. Am. Chem. Soc., 103,* 4927 (1981).
6 Y. Huang and R. J. Kassner, *J. Biol. Chem., 256,* 5327 (1981).
7 G. McLendon and M. Smith, *J. Am. Chem. Soc., 103,* 4912 (1981).
8 G. McLendon and M. Smith, *Inorg. Chem., 21,* 847 (1982).
9 H. A. Harburg and P. A. Loach, *J. Biol. Chem., 235,* 3640 (1960).
10 H. Gray, in A. Addison (ed.), 'Biological Aspects of Inorganic Chemistry', Wiley, New York, 1979, p. 289.
11 A. G. Sykes, E. Margoliash, J. Butler, D. M. Davies, W. H. Koppenol and N. Osherhoff, *J. Am. Chem. Soc., 103,* 469 (1981).
12 G. McLendon and M. Smith, *J. Am. Chem. Soc., 102,* 566 (1980).
13 E. M. Roberts and W. S. Koski, *J. Chem. Phys., 34,* 591 (1961).
14 C. P. S. Taylor, *Biochim. Biophys. Acta, 491,* 137 (1977).
15 J. C. Salermo and J. S. Leigh, *J. Am. Chem. Soc., 106,* 2156 (1984).
16 M. Iwaisumi and C. T. Migita, *J. Am. Chem. Soc., 103,* 4378 (1981).

17 I. Salmeen and G. Plamer, *J. Chem. Phys., 48,* 2049 (1968).
18 J. S. Griffith, *Nature (London), 180,* 30 (1957).
19 G. Harris, *Theor. Chim. Acta (Berlin), 5,* 379 (1966).
20 B. Muhoberac, *Arch. Biochem. Biophys., 233,* 682 (1984).
21 J. Peisach, W. E. Blumberg and A. Adler, *Ann. N.Y. Acad. Sci., 206,* 310 (1973).
22 W. E. Blumberg and J. Peisach, in B. Chance, T. Yonetani and A. Mildvar (eds.), 'Structure and Function of Macromolecules and Membranes', Vol. 2, Academic Press, New York, 1971.
23 (a) A. S. Brill and R. J. R. Williams, *Biochem. J., 78,* 246 (1961); (b) R. J. Williams and D. W. Smith, *Struct. Bonding (Berlin), 7,* 1 (1970).
24 (a) M. Gouterman, H. Kobayashi and M. Zerner, *Theor. Chim. Acta (Berlin), 6,* 363 (1966); (b) M. Gouterman, in D. Dolphin (ed.), 'The Porphyrins', Vol. III, Academic Press, New York, 1978, Chap. 1.
25 W. E. Blumberg, in A. Ehrenberg, G. Malstrom and T. Vanngard (eds.), 'Magnetic Resonance in Biological Systems', Pergamon, Oxford, 1967, p. 119.
26 T. Bohan, *J. Magn. Reson., 26,* 109 (1977).
27 J. Shack and W. M. Clark, *J. Biol. Chem., 171,* 143 (1947).
28 R. G. Little, K. R. Dymock and J. A. Ibers, *J. Am. Chem. Soc., 97,* 4532 (1975).
29 J. F. Deathridge, R. S. Loe, C. M. Anderson and K. Moffat, *J. Mol. Biol., 104,* 687 (1976).
30 J. F. Deathridge, S. K. Obendorf and K. Moffat, *J. Mol. Biol., 134,* 419 (1979).
31 J. S. Griffith, *Biopolymers Symp., 1,* 35 (1964).
32 J. F. Gibson and D. J. E. Ingram, *Nature (London), 180,* 29 (1959).
33 M. F. Perutz, *Nature (London), 228,* 726 (1970).
34 J. W. Buchler, in K. Smith (ed.), 'Porphyrins and Metalloporphyrins', Elsevier, Amsterdam, 1975, p. 157.
35 C. J. O'Connor, *Prog. Inorg. Chem., 29,* 203 (1982).
36 W. A. Eaton and R. M. Hochstrasser, *J. Chem. Phys., 49,* 985 (1968).
37 W. A. Eaton, L. K. Hanson, P. J. Stephens, J. C. Sutherland and J. B. R. Dunn, *J. Am. Chem. Soc., 100,* 4991 (1978).
38 A. K. Makinen and M. W. Churg, *J. Chem. Phys., 68,* 1913 (1978).
39 M. W. Makinen and A. K. Churg, in A. B. P. Lever and H. Gray (eds.), 'Iron Porphyrins' Part One, Elsevier, New York, 1983, p. 141.
40 A. C. Anusiem, J. G. Beetlestone and D. H. Irvine, *J. Chem. Soc. A,* 357 (1966).
41 P. George and J. Ilzaka, *Biochem. Biophys. Acta, 393,* 335 (1975).
42 H. Hori and H. Hiroshi, *Biochem. Biophys. Acta, 251,* 227 (1971).
43 J. Peisach and W. E. Blumberg, *J. Biol. Chem., 262,* 5859 (1977).
44 W. Scheler and F. Jung, *Biochem. Z., 325,* 515 (1954).
45 M. Ikeda-Saito and T. Ilzuka, *Biochem. Biophys. Acta, 393,* 335 (1975).
46 P. George and C. L. Tsou, *Biochem. J., 50,* 440 (1952).
47 E. Margoliash, N. Frehwirt and E. Wiener, *Biochem. J., 71,* 559 (1959).